

FABRICATION AND MAGNETIC PROPERTIES OF SINTERED $\text{SrFe}_{12}\text{O}_{19}$ - NiFe_2O_4 NANOCOMPOSITES

TRAN THI VIET NGA[†] AND TO THANH LOAN

*International Training Institute for Materials Science (ITIMS) Hanoi University of Technology,
01 Dai Co Viet Street, Hanoi, Vietnam*

[†]E-mail: vietnga@itims.edu.vn

Received 22 July 2017

Accepted for publication 07 September 2017

Published 19 September 2017

Abstract. *Two series of $\text{SrFe}_{12}\text{O}_{19}/\text{NiFe}_2\text{O}_4$ nanocomposite ferrites sintered in air at 850°C and 950°C were prepared using $\text{SrFe}_{12}\text{O}_{19}$ and NiFe_2O_4 nanopowders obtained via sol-gel method. The phase composition, surface morphology and magnetic properties of the composites were investigated using XRD, SEM and VSM respectively. For the $\text{SrFe}_{12}\text{O}_{19}/\text{NiFe}_2\text{O}_4$ ferrites with volume ratio ranging from 61 to 21 and sintered in 850°C for 5 hours in air, all the specimens are composed of two phases but exhibit a typical single-phase magnetic behavior, indicating the existence of exchange coupling (EC) between the magnetically hard and soft phases. The value of coercivity H_c decreases from 6.19 kOe to 0.574 kOe when volume of $\text{SrFe}_{12}\text{O}_{19}$ decreases from 6 to 1. While the samples with a mass ratio of $R_m = \text{SrFe}_{12}\text{O}_{19}/\text{NiFe}_2\text{O}_4$ varying from 31 to 13 sintered in 950°C for 5 hours characterized with a “bee waist” type hysteresis loop. These results reveal that the magnetically hard and soft magnetic phases are not exchange-coupled. The saturation magnetization (M_S) increases from 36 emu/g to 43.3 emu/g when R_m decreases from 31 to 13 and then decreases with $R_m = 12$ and 13.*

Keywords: Magnetic properties, nano structure.

Classification numbers: 74.78.Na; 75.75.-c.

I. INTRODUCTION

In recent years, nanocomposite magnets have attracted considerable attentions due to their potential applications in microwave devices [1], high-density magnetic recording [2], electronic devices and magnetofluid medicine [3]. Theoretically, by combining high magnetic anisotropy of a magnetically hard phase and the high saturation magnetization of magnetically soft phase, exchange-coupled composite permanent magnets can enhanced magnetic properties of the ferrites [4]. The hexagonal ferrites have high coercivity, large anisotropy field [5] and the spinel ferrites have high saturation at room temperature [4]. They both have good mechanical, chemical stability and high microwave magnetic loss [4, 7]. Recently, many researchers have paid much attention in studies of ferrite composite powders including hexagonal and spinel ferrites. However, the magnetic properties of the ferrite composite powders are highly sensitive to grain size, microstructure, distribution of the magnetically hard and soft phases, as well as impurity [4]. Therefore, to achieve highly homogeneous ferrite particles, low-temperature chemical methods have been used, such as hydrothermal [8, 9], sol-gel [10, 11]. Moreover, the ferrites can be successfully synthesized at a relatively low temperature without sintering at high temperatures, which may be beneficial to control the growth of crystallites. Some results on nanocomposite particles can be mentioned as: BaM + χ vol% $\text{Ni}_{0.5}\text{Zn}_{0.5}\text{Fe}_2\text{O}_4$ [12], SrM/ $\text{Ni}_{0.7}\text{Zn}_{0.3}\text{Fe}_2\text{O}_4$ [13], $\text{BaCa}_2\text{Fe}_{16}\text{O}_{27}/\text{Fe}_3\text{O}_4$ [14], $\text{SrFe}_{12}\text{O}_{19}/\text{CoFe}_2\text{O}_4$ [15], $\text{BaFe}_{12}\text{O}_{19}/\text{CoFe}_2\text{O}_4$ [16],... As reported, the saturation magnetization is enhanced markedly with the increase of magnetically soft phase content. For the $\text{SrFe}_{12}\text{O}_{19}/\text{CoFe}_2\text{O}_4$ particles, an enhancement of 25% in saturation magnetization can be achieved with the decrease of $R_m = \text{SrFe}_{12}\text{O}_{19}/\text{CoFe}_2\text{O}_4$ ratio from 3/1 to 1/3.

In this work, two series of $\text{SrFe}_{12}\text{O}_{19}/\text{NiFe}_2\text{O}_4$ nanocomposite powders with different mass and volume ratios were prepared by sol-gel method and their structural, morphology and magnetic properties were studied.

II. EXPERIMENT

II.1. Synthesis of $\text{SrFe}_{12}\text{O}_{19}$ and NiFe_2O_4 powders

$\text{SrFe}_{12}\text{O}_{19}$ and NiFe_2O_4 nanopowders were synthesized separately by via sol-gel method. $\text{Fe}(\text{NO}_3)_3 \cdot 9\text{H}_2\text{O}$, $\text{Sr}(\text{NO}_3)_2$ and $\text{Ni}(\text{NO}_3)_2 \cdot 6\text{H}_2\text{O}$ were dissolved in deionized water to form an aqueous solution of 1M. The nitrates used to synthesize $\text{SrFe}_{12}\text{O}_{19}$ and NiFe_2O_4 were dissolved in deionized water with the molar ratio Sr/Fe is 12 and Ni/Fe is 2. Citric acid (AC) was then added into the solution at fixed $[\text{Sr}^{2+} + \text{Fe}^{3+}]:\text{AC}$ and $[\text{Ni}^{2+} + \text{Fe}^{3+}]:\text{AC}$ molar ratio of 1:3. NH_4OH was used to adjust the pH to 1. After the pH had been stabilized, the solution was stirred at 1000 rpm and gradually evaporated at 90°C . As the water evaporated, the remainder became highly viscous gels with brown color as a result of the chelation process. These gels were dried at 90°C for 24 h, and then heated at 450°C for 2 h to eliminate the remaining residual water and other organic impurities (aerogels were formed). To form the hexaferrite and spinel phase, the gels were calcined in air at 850°C for 5 hours.

II.2. Preparation of $\text{SrFe}_{12}\text{O}_{19}/\text{NiFe}_2\text{O}_4$ nanocomposites

The first series of specimens $\text{SrFe}_{12}\text{O}_{19}/\text{NiFe}_2\text{O}_4$ nanopowders were synthesized using the aerogel powders obtained previously. $\text{SrFe}_{12}\text{O}_{19}$ and NiFe_2O_4 aerogel powders were uniformly mixed with mass ratios (R_m) of 3:1, 3:2, 1:2, 1:3 and 1:1, denoted as $R_m = 31, 32, 33, 12$ and 13,

respectively. Then the mixtures were pressed into platelets of 6 mm in diameter and sintered at 950 °C for 5 hours.

The second series of specimens, The $\text{SrFe}_{12}\text{O}_{19}/\text{NiFe}_2\text{O}_4 = R_V$ ($R_V = 6:1$, step 1:1) nanocomposite powders were synthesized by one step sol-gel method. Stoichiometric amounts of $\text{Fe}(\text{NO}_3)_3 \cdot 9\text{H}_2\text{O}$, $\text{Sr}(\text{NO}_3)_2$, $\text{Ni}(\text{NO}_3)_2$ were dissolved completely in deionized water. In these processes, the ratio of $\text{Sr}^{2+}/\text{Fe}^{3+}$ and $\text{Fe}^{3+}/\text{Ni}^{2+}$ were fixed at 12 and 2. Citric acid was then added into the solution at a fixed $(\text{Sr}^{2+} + \text{Fe}^{3+} + \text{Ni}^{2+})/\text{AC}$ volume ratio of 1/3. NH_4OH in aqueous form was added to the mixed solutions and the pH of the solutions was adjusted to about 1. The mixtures were stirred at 1000 rpm and slowly evaporated at 90 °C to form gels. These gels were dried at 90 °C for 24 h, and then heated at 450 °C for 2 hours to eliminate the remaining residual water and other organic impurities. An equal weight of the produced ferrite powders were compressed into briquettes of 6 mm diameters and 3 g weight. The composites were annealed in air at 850 °C for 5 h. This samples were denoted as $R_V = 61, 51, 41, 31, 21$ and 11.

II.3. Characterization

The crystal structure and phases of the obtained samples were identified via X-ray powder diffraction (XRD) using a Siemens D5000 diffractometer ($\text{CuK}\alpha$ radiation, $\lambda = 1.54056 \text{ \AA}$). Morphological features and particle size were observed by scanning electron microscopy (SEM, JEOL-JSM 7600F). The magnetic were measured using a vibrating sample magnetometer (VSM, Lakeshore 7410) with applied magnetic fields up to 17 kOe.

III. RESULTS AND DISCUSSIONS

The XRD patterns of the $\text{SrFe}_{12}\text{O}_{19}/\text{NiFe}_2\text{O}_4$ nanocomposite powders with various ratios of R_m and R_V are shown in Fig. 1. It can be clearly seen that only the parent phases of $\text{SrFe}_{12}\text{O}_{19}$ and NiFe_2O_4 can be found in all samples. The diffraction peaks can be indexed to the hexagonal magnetoplumbite structure of $\text{SrFe}_{12}\text{O}_{19}$ and the cubic spinel structure of NiFe_2O_4 without any impurity phase, suggesting that all the specimens are composed of NiFe_2O_4 and $\text{SrFe}_{12}\text{O}_{19}$ phases after annealing. As shown in Fig. 1, the relative intensity of peaks from NiFe_2O_4 enhanced with the decrease of R_m and R_V , which indirectly proves the content increasing of NiFe_2O_4 in composites. The ratio of intensity of the strongest peaks from $\text{SrFe}_{12}\text{O}_{19}$ and NiFe_2O_4 in Fig. 1 as α :

$$\alpha = I_{\text{SrFe}_{12}\text{O}_{19}}^{(114)} / I_{\text{NiFe}_2\text{O}_4}^{(311)} \quad (1)$$

where $I_{\text{SrFe}_{12}\text{O}_{19}}^{(114)}$ and $I_{\text{NiFe}_2\text{O}_4}^{(311)}$ are the intensity of the (114) and (311) peaks for $\text{SrFe}_{12}\text{O}_{19}$ and NiFe_2O_4 phase, respectively. The values of α for composite samples with different ratios R_m and R_V are listed in Table 1. The value of α for $R_m = 31, 32, 33, 12$ and 13 decreases from 0.97 to 0.2 in Fig. 2b, while the value of α for $R_V = 61, 51, 41, 31$ increases from 1.18 to 1.63 and decreases with $R_V = 21$ and 11 in Fig. 2a. Moreover, no unrecognized peak is found in Fig. 2, suggesting that no impurity phase was formed in the composites after sintering.

Figures 2a and 2b give the SEM images of the NiFe_2O_4 and $\text{SrFe}_{12}\text{O}_{19}$ samples calcinated at 850 °C for 2 h, respectively. It can be seen that the NiFe_2O_4 and $\text{SrFe}_{12}\text{O}_{19}$ particles has a proper cubic and hexagonal platelet shape. The average paricle sizes of NiFe_2O_4 and $\text{SrFe}_{12}\text{O}_{19}$ were evenly distributed in the range of 30 - 60 nm and 80 - 100 nm, respectively.

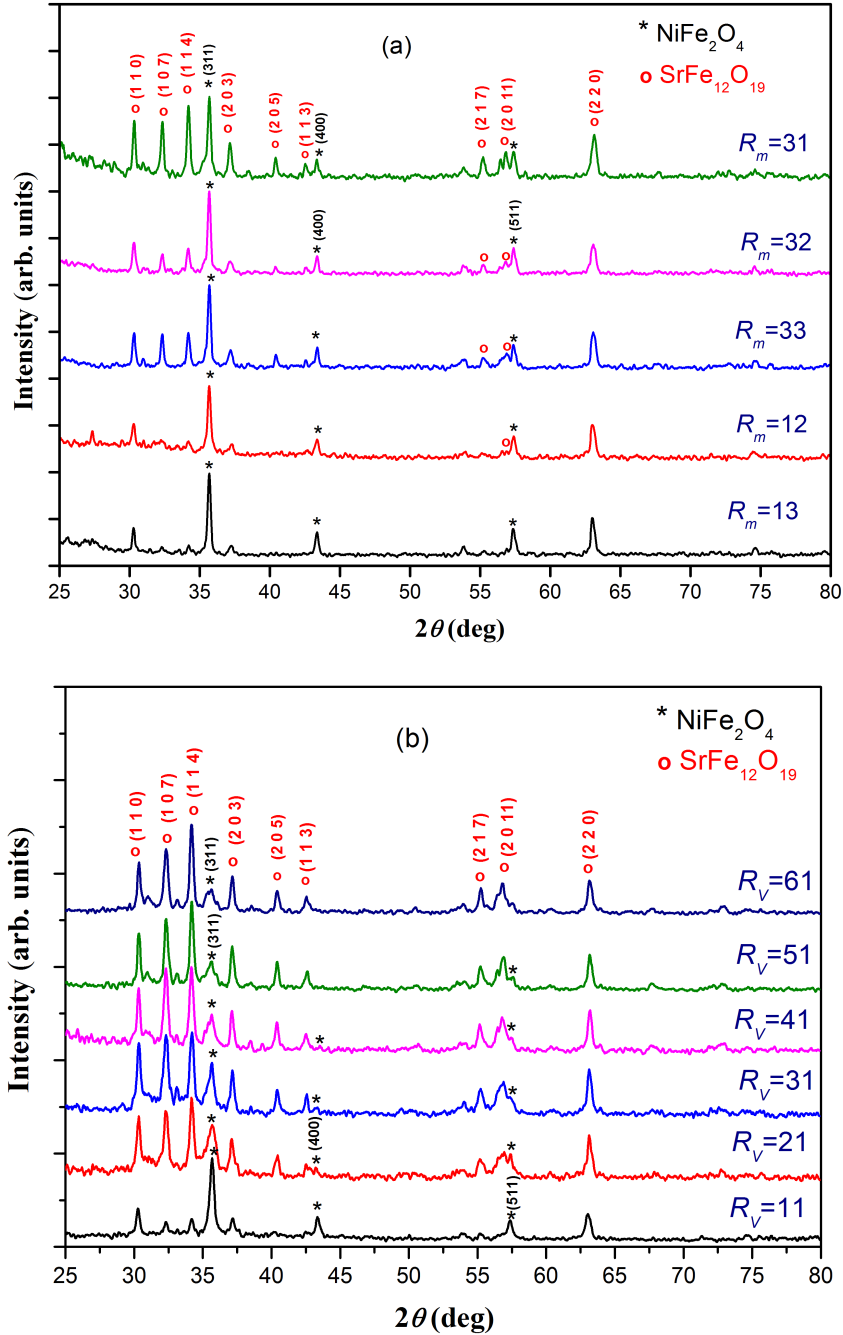


Fig. 1. XRD patterns of the $\text{SrFe}_{12}\text{O}_{19}/\text{NiFe}_2\text{O}_4$ nanocomposite powders (a) with different R_m calcination at 950°C and (b) with different R_v calcination at 850°C for 5 hours.

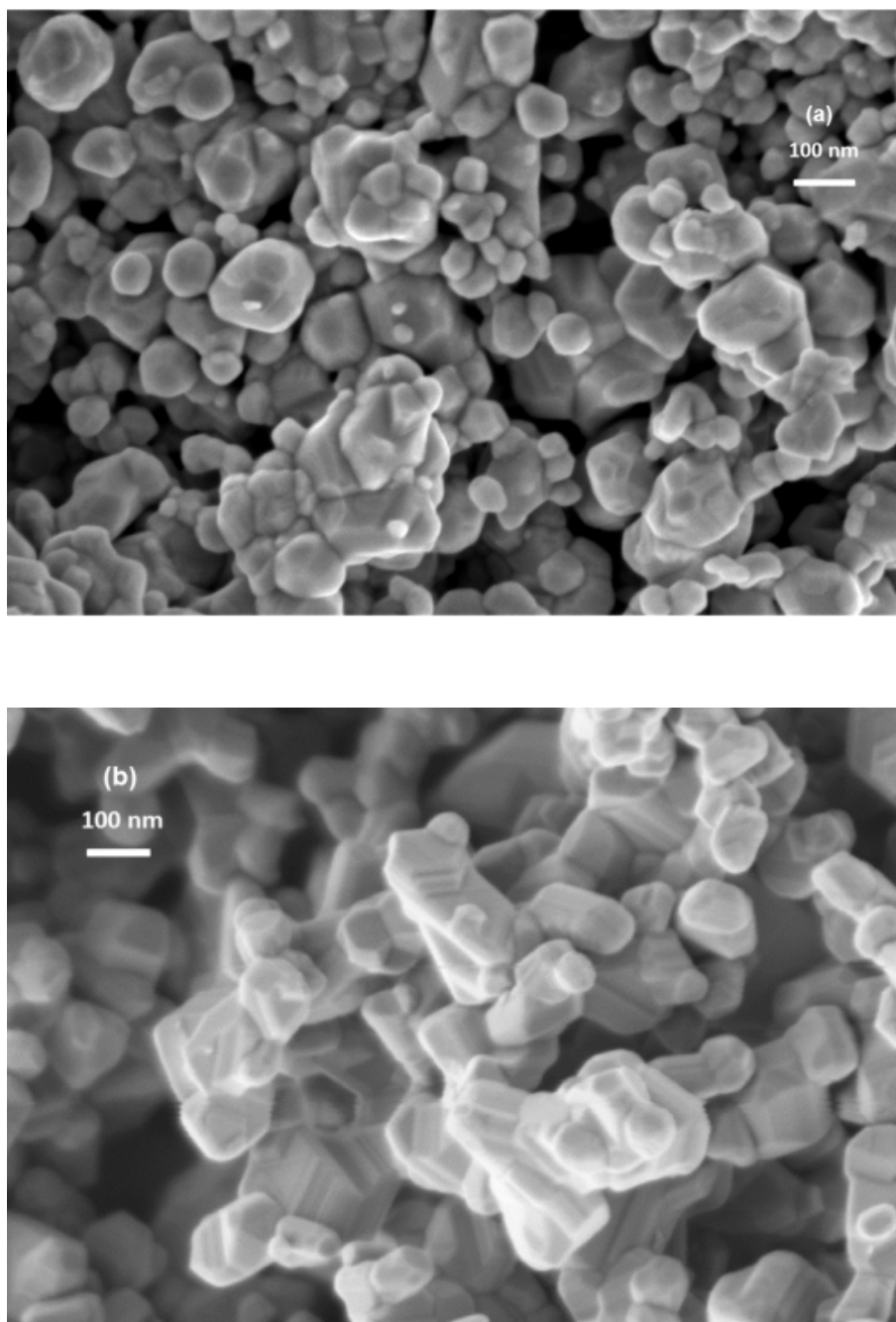


Fig. 2. SEM images of the NiFe₂O₄ (a) and SrFe₁₂O₁₉ (b) particles calcinated at 850 °C for 5 hours.

Table 1. Results obtained from XRD analysis: lattice parameters a, c and the $\alpha = I_{\text{SrFe}_{12}\text{O}_{19}}^{(114)} / I_{\text{NiFe}_2\text{O}_4}^{(311)}$ ratios of the $\text{SrFe}_{12}\text{O}_{19}/\text{NiFe}_2\text{O}_4$ nanocomposite powders with different ratios R_m, R_V .

<i>Composition</i>	<i>Phase</i>	a (Å)	c (Å)	$\alpha = \frac{I_{\text{SrFe}_{12}\text{O}_{19}}^{(114)}}{I_{\text{NiFe}_2\text{O}_4}^{(311)}}$
$R_V = 61$	$\text{SrFe}_{12}\text{O}_{19}$	5.874	23.026	1.18
	NiFe_2O_4	8.308		
$R_V = 51$	$\text{SrFe}_{12}\text{O}_{19}$	5.873	23.015	1.21
	NiFe_2O_4	8.313		
$R_V = 41$	$\text{SrFe}_{12}\text{O}_{19}$	5.873	23.016	1.21
	NiFe_2O_4	8.313		
$R_V = 31$	$\text{SrFe}_{12}\text{O}_{19}$	5.873	23.016	1.63
	NiFe_2O_4	8.313		
$R_V = 21$	$\text{SrFe}_{12}\text{O}_{19}$	5.869	23.016	1.25
	NiFe_2O_4	8.323		
$R_V = 11$	$\text{SrFe}_{12}\text{O}_{19}$	5.873	23.013	0.34
	NiFe_2O_4	8.326		
$R_m = 31$	$\text{SrFe}_{12}\text{O}_{19}$	5.8752	23.0170	0.97
	NiFe_2O_4	8.3316		
$R_m = 32$	$\text{SrFe}_{12}\text{O}_{19}$	5.8756	23.0175	0.83
	NiFe_2O_4	8.3315		
$R_m = 33$	$\text{SrFe}_{12}\text{O}_{19}$	5.8757	23.0173	0.8
	NiFe_2O_4	8.3312		
$R_m = 12$	$\text{SrFe}_{12}\text{O}_{19}$	5.8755	23.0172	0.68
	NiFe_2O_4	8.3314		
$R_m = 13$	$\text{SrFe}_{12}\text{O}_{19}$	5.8757	23.0171	0.2
	NiFe_2O_4	8.3313		

The hysteresis loops of the $\text{SrFe}_{12}\text{O}_{19}$ and NiFe_2O_4 powders are shown in the Fig. 3. It is clearly seen that the phases $\text{SrFe}_{12}\text{O}_{19}$ ferrite and NiFe_2O_4 ferrite are correspondingly characterized with the magnetically hard and soft material, respectively. The intrinsic coercivity (H_c) reached 7 kOe and 0.134 kOe for $\text{SrFe}_{12}\text{O}_{19}$ and NiFe_2O_4 samples, respectively.

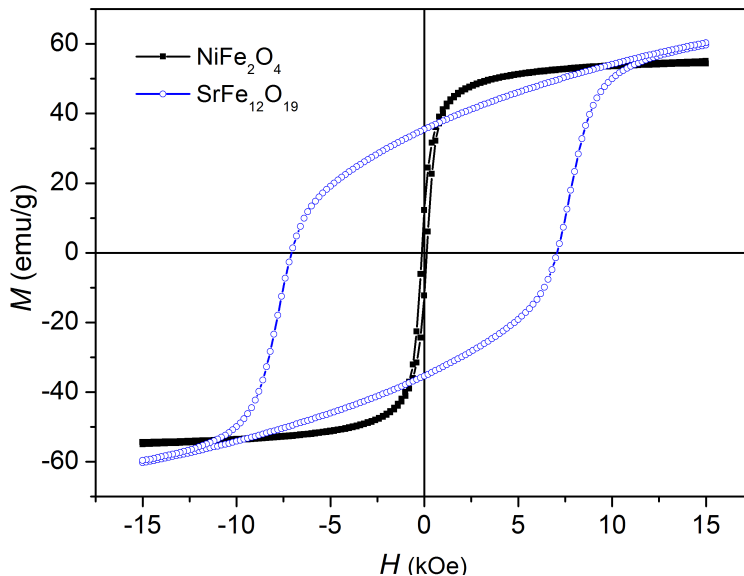


Fig. 3. Hysteresis loops of the $\text{SrFe}_{12}\text{O}_{19}$ and NiFe_2O_4 magnets annealed at 850°C for 2 h.

In order to analyze the effect of fabrication methods and the ratio of $\text{SrFe}_{12}\text{O}_{19}:\text{NiFe}_2\text{O}_4$ on the particle sizes and particle size distributions, the SEM images of composite samples after calcination were carried out and these images are presented in Fig. 4 and 5. Figure 4 shows SEM micrographs of composite samples with $R_m = 31, 11, 12$ and 13 . As can be seen from these figures, samples consist of cubic grains and hexagonal plate-like grains. However the distribution of particles are not almost homogeneous. The cubic grains with smaller size lie on the face of hexagonal grains with larger size and the particles are agglomerated. The agglomeration of nanoparticles may be due to the magnetic interactions between them. With increasing the concentration of NiFe_2O_4 , the grains size of soft phase increases from 20 nm to 40 nm while the grains size of $\text{SrFe}_{12}\text{O}_{19}$ phase are less increase. The hexagonal plate-like grains have approximate diameter from 50 nm to 100 nm. These results were in agreement with those reported by Miao Liu *et al.* [16]. In this study, the $\text{BaFe}_{12}\text{O}_{19}/\text{CoFe}_2\text{O}_4$ nanocomposite powders were also prepared by sol-gel method and calcined at 1000°C . The samples consist two phases and the grain size is about 100 - 250 nm. Figure 5 shows SEM micrographs of composite samples with $R_V = 41, 31, 21$ and 11 . It can be found that the two phases are homogeneous distributed and the grain size of the composite powders is about 30 - 50 nm. For the sample with $R_V = 21$ and 11 , it can be clearly seen that the nanocomposite powders are built from $\text{SrFe}_{12}\text{O}_{19}$ and NiFe_2O_4 , in which the grains size of hard phase increases with increasing the concentration of NiFe_2O_4 .

The magnetic properties such as magnetization at 1.5T (M), remanence magnetization (M_r) and coercivity (H_C) are calculated from the hysteresis loops (Fig. 6) measured at room temperature and results are listed in Table 2. As seen in the Fig. 6a, for all samples, the stepped hysteresis loops can be indicated that two independent magnetic phases are co-existed. These magnetic properties results were in agreement with the XRD results in Fig. 1a. Therefore, this mechanical mixing method is an inadequate method for obtaining exchange-spring magnets because of non-homogeneously distributed soft and hard magnetic phases. As expected, with increasing the concentration of NiFe_2O_4 the coercivity (H_C) decreases. It may be due to the fact the H_C of NiFe_2O_4 is smaller than that of $\text{SrFe}_{12}\text{O}_{19}$. The H_C reduction is also achieved when increasing the soft phase concentration in Ba-hexaferrite/NiZn ferrite nanocomposites samples [12]. The value of M increases steeply with the increase of NiFe_2O_4 concentration (from $R_m=31$ to 33), reaches the maximum value of 43.3 emu/g at $R_m = 33$, and decreases at $R_m = 12$ and 13. This is due to the particles distribution and magnetic interactions between them (Fig. 4c and Fig. 4d).

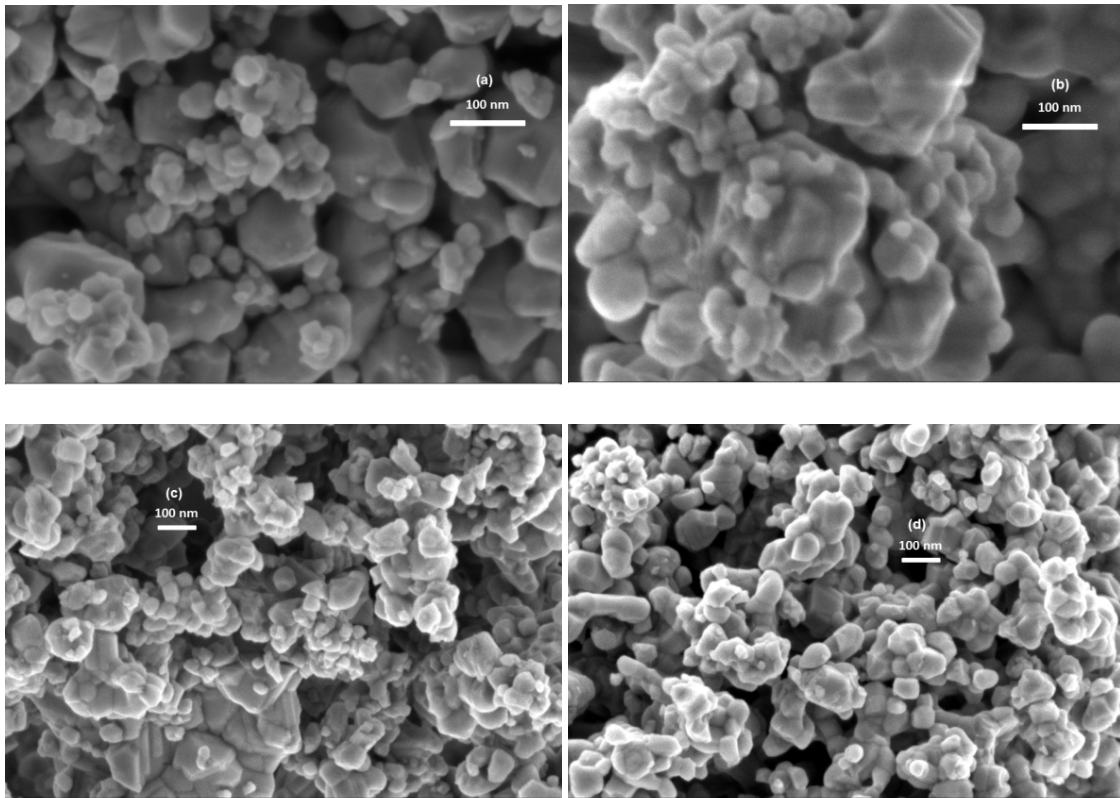


Fig. 4. SEM images of the $\text{SrFe}_{12}\text{O}_{19}/\text{NiFe}_2\text{O}_4$ nanocomposite samples with different mass ratios (R_m): (a) $R_m=31$, (b) $R_m=11$, (c) $R_m=12$ and (d) $R_m=13$ calcinated at 950°C for 5 h.

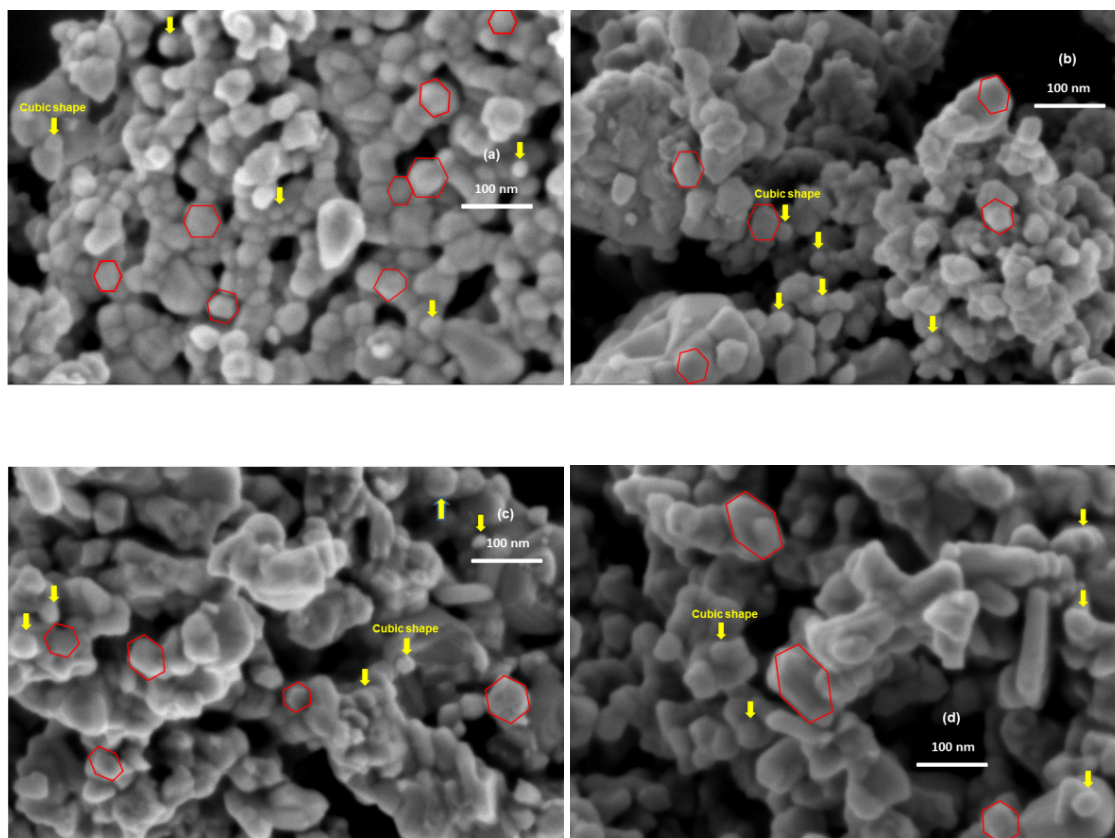


Fig. 5. SEM images of the $\text{SrFe}_{12}\text{O}_{19}/\text{NiFe}_2\text{O}_4$ nanocomposite samples with different volume ratios (R_V): (a) $R_V=41$, (b) $R_V=31$, (c) $R_V=21$ and (d) $R_V=11$ calcinated at 850°C for 5 h.

The samples with the ratios of $R_V = 61, 51, 41, 31, 21$ exhibit an excellent smooth hysteresis loop and show a single-phase magnetization behavior, although they are crystallographically composed of two phase. It indicated that the hard and soft magnetic phases are well exchange-coupled [16–18]. Meanwhile the sample with $R_V = 11$ is characterized with a “bee waist” type hysteresis loop, implying that the hard and soft magnetic phases are not exchange-coupled. The magnetic parameters M_s , M_r and H_c observed from Fig. 6b are listed in Table 2. It is also clearly seen that the value of coercivity H_c markedly decreases from 6.19 kOe to 0.574 kOe when volume of $\text{SrFe}_{12}\text{O}_{19}$ decreases from 6 to 1. The value of the magnetization M increases 0.8% when R_V decreases from 61 to 51, and then decreases greatly with decreasing volume of $\text{SrFe}_{12}\text{O}_{19}$. This results was mainly attributed to the fact the H_c and M_s of NiFe_2O_4 are lower than those of $\text{SrFe}_{12}\text{O}_{19}$. Theoretically, there are two main interactions, exchange and dipolar interactions, that determine the magnetic properties of nanoparticles which are combined from magnetically hard and soft phases. If the soft phase is neglected, direct coupling among hard grains is controlled by magnetostatic energy due to the dipolar interaction between hard grains. When the presence of the soft, the direct

coupling of the hard grains decreases. With the samples having low concentrations of soft phase, the exchange interaction on the moments of soft phase defecated by the hard phase is strong, hence the coercive field increases. With increasing the concentration of soft phase, the exchange interaction between the hard and soft grains would be weakened and dipolar interaction among soft phases is enhanced. Therefore, the coercivity decreases with increasing concentration of NiFe_2O_4 [19]. These phenomenon also observed for the $\text{BaFe}_{12}\text{O}_{19}/\text{CoFe}_2\text{O}_4$ [11], $\text{BaFe}_{12}\text{O}_{19}/\text{NiZnFe}_2\text{O}_4$ [4] and $\text{SrFe}_{12}\text{O}_{19}/\text{CoFe}_2\text{O}_4$ [10]. Meanwhile, the decrease in saturation magnetization can be also explained based on grain size, particles distribution, spin canting, and impurity. The magnetic parameters such as M , M_r and H_C of nanocomposite samples with different R_V are higher than those of nanocomposite samples with different R_m . These results were mainly attributed to improvement in crystalline and two phases homogeneity using solution mixing method.

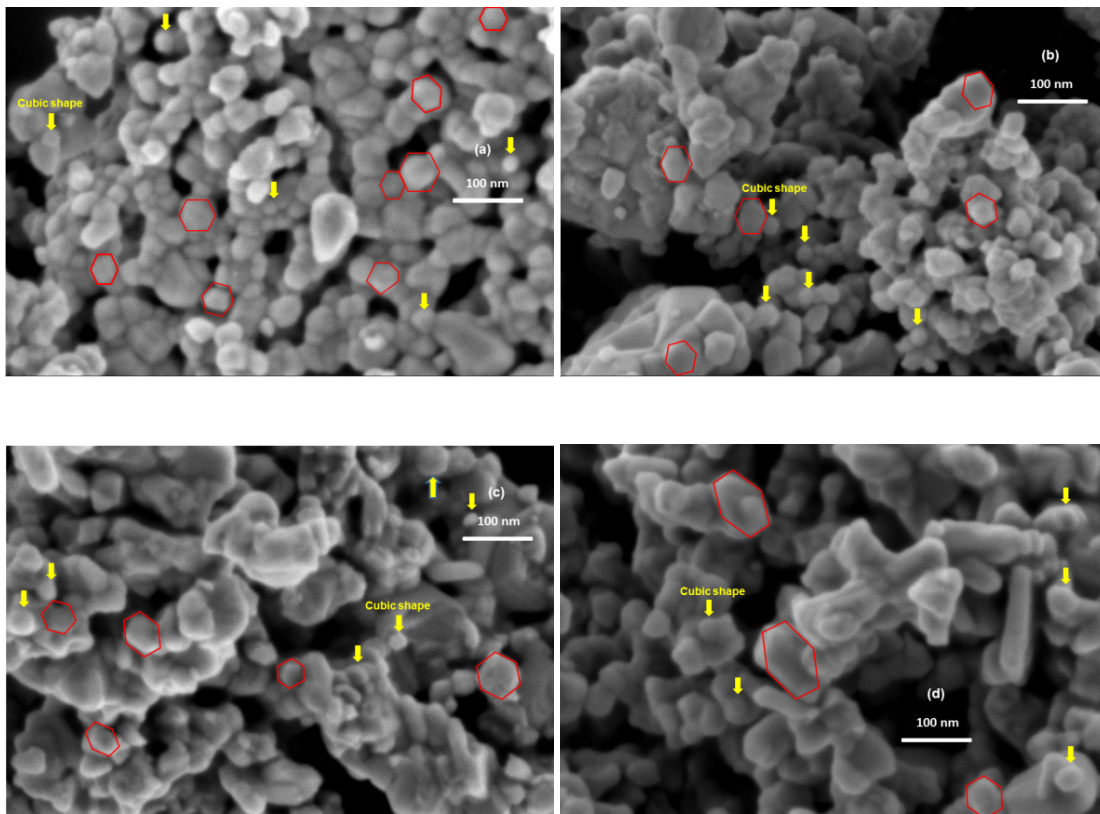


Fig. 6. Hysteresis loops of the $\text{SrFe}_{12}\text{O}_{19}/\text{NiFe}_2\text{O}_4$ nanocomposite samples (a) with different R_m calcination at 950°C and (b) with different R_V calcination at 850°C for 5 hours.

IV. CONCLUSION

In summary, it is the first time $\text{SrFe}_{12}\text{O}_{19}/\text{NiFe}_2\text{O}_4$ nanocomposite powders with different mass and volume ratios (R_m and R_V) were successfully prepared by the sol-gel method. It is found

Table 2. Magnetization at 1.5T (M) and coercive force (H_c) and remanence magnetization (M_r) at room temperature of the SrFe₁₂O₁₉/NiFe₂O₄ nanocomposite powders with different ratios R_m , R_V .

Composition	M (emu/g)	H_c (kOe)	M_r (emu/g)
SrFe ₁₂ O ₁₉	60	7	35.14
NiFe ₂ O ₄	55	0.134	13.6
$R_V = 61$	51.19	6.19	30.81
$R_V = 51$	51.56	6.17	31.05
$R_V = 41$	50.76	5.68	30.81
$R_V = 31$	50.42	5.1	30.08
$R_V = 21$	51.28	4.09	30.08
$R_V = 11$	42.58	0.574	15.08
$R_m = 31$	34	5.3	14
$R_m = 32$	38.5	2.3	17.52
$R_m = 33$	43.3	2.3	20.87
$R_m = 12$	37.6	0.36	12.40
$R_m = 13$	0.36	0.22	12.37

that the specimens with mass ratios $R_V = 61, 51, 41, 31$ and 21 after sintering at 850°C for 5 h exhibit magnetically single phase, indicating the existence of exchange coupling between magnetically hard and soft phases. The value of coercivity H_c and magnetization at 1.5T M decrease with the increase of the volume NiFe₂O₄. Compared with the SrFe₁₂O₁₉ ferrite, coercivity H_c and magnetization M are reduced markedly with the increase of NiFe₂O₄ content. These results also indicate that mechanical mixing method is an inadequate method for obtaining exchange coupling in the different mass ratios R_m samples because of non-homogeneously distributed soft and hard magnetic phases. Though the exchange coupling interaction reduces the coercivity of SrFe₁₂O₁₉ phase, it can enhance the magnetization and the coercivity of NiFe₂O₄ phase.

ACKNOWLEDGMENT

The Current work was financially supported by Hanoi University of Science and Technology (Grant No. T2016-PC-130).

REFERENCES

- [1] Y. H. Liu, S. G. E. te Velthuis, J. S. Jiang, Y. Choi, S. D. Bader, A. A. Parizzi, H. Ambaye, V. Lauter, *Phys. Rev. B* **83** (2011) 174418.
- [2] S. E. Jacobo, L. Civalo, M.A. Blesa, *J. Magn. Magn. Mater.* **37** (2000) 260.
- [3] Y. F. Lu, W. D. Song, *Appl. Phys. Lett.* **76** (2000) 490.
- [4] M. A. Moskalenko, V. M. Uzdin, H. Zabel, *J. Appl. Phys.* **115** (2014) 053913.
- [5] P. C. Pullar, *Prog. Mater. Sci.* **57** (2012) 1191.
- [6] T. Nakamura, *J. Appl. Phys.* **88** (2000) 348.
- [7] X. F. Pan, J. X. Qiu, M. Y. Gu, *J. Mater. Sci.* **42** (2007) 2086
- [8] A.L. Xia, C.H. Zuo, L. Chen, C.G. Jin and Y.H. Lv, *J. Magn. Magn. Mater.* **332** (2013) 186-191.
- [9] A. L. Xia, X. Z. Hu, D. K. Li, L. Chen, C. G. Jin, C. H. Zuo and S. B. Su, *Electron. Mater. Lett.* **10** (2014) 423.

- [10] B. N. Pianciola, E. Lima Jr., H. E. Troiani, L. C. C. M. Nagamine, R. Cohen, R. D. Zysler, *J. Magn. Magn. Mater.* **377** (2015) 44-51.
- [11] C. N. Chinnasamy, B. Jeyadevan, K. Shinoda, K. Tohji, D.J. Djayaprawira, M. Takahashi, R. J. Joseyphus, A. Narayanasamy, *Appl. Phys. Lett.* **83** (2003) 2862.
- [12] K. W. Moon, S. G. Cho, Y. H. Choa, K. H. Kim and J. Kim, *Phys. Status Solidi a* **204** (2007) 4141.
- [13] M. A. Radmanesh, S. A. S. Ebrahimi, *J. Magn. Magn. Mater.* **324** (2012) 3094.
- [14] D. Roy, P.S.A. Kumara, *J. Appl. Phys.* **106** (2009) 073902.
- [15] L.Y. Zhang, Z.W. Li, *J. Alloys Compd.* **469** (2009) 422.
- [16] Haibo Yang, Miao Liu, Ying Lin, Guoqiang Dong, Lingyan Hu, Ying Zhang, Jingyi Tan, *Mater. Chem. Phys.* **160** (2015) 5.
- [17] Y. H. Liu, S. G. E. T. Velthuis, J. S. Jiang, Y. Choi, S. D. Bader, A. A. Parizzi, H. Ambaye, V. Lauter, *Phys. Rev. B* **83** (2011) 174418.
- [18] Ailin Xia, Suzhen Ren, Junshu Lin, Yue Ma, Chen Xu, Jinlin Li, Chuangui Jin, Xianguo Liu, *J. Alloys Compd.* **653** (2015) 108.
- [19] H. Zeng, S. H. Sun, J. Li, Z. L. Wang, J. P. Liu, *Appl. Phys. Lett.* **85** (2004) 792.